SUPPLEMENTAL ONLINE INFORMATION.

Individual motile CD4^{+} T cells can participate in efficient multi-killing through conjugation to multiple tumor cells

Ivan Liadi, Harjeet Singh, Nicolas Rey-Villamizar, Gabrielle Romain, Amin Merouane, Jay R T. Adolacion, Partow Kebriaei, Helen Huls, Peng Qiu, Badrinath Roysam, Laurence J.N. Cooper, Navin Varadarajan

Glossary of terms used in the paper

| CAR	Chimeric Antigen Receptor
E	Effector CAR^+ T-cell
T	Target cell
CRA	^{51}Chromium Release Assay (population level assay)
AICD	Activation Induced Cell Death
ACT	Adoptive Cell Therapy
aAPC	Artificial antigen presenting cells
TIMING	Timelapse Imaging Microscopy In Nanowell Grids
Multi-killing	Ability of a single T-cell to kill two or more target cells
N_{total}	Total number of events
CAR4 cell	$CD4^+CAR^+$ T-cell
CAR8 cell	$CD8^+CAR^+$ T-cell
Killing frequency	Number of T cells capable of participating in killing
Killing efficiency	Description of the kinetics of killing mediated by individual T cells (Please see t_{Death} below)
Conjugation	Stable contact between effector cell and target cell lasting > 7 minutes
t_{Seek}	Time taken by T-cell to conjugate with tumor cell
t_{Death}	Time elapsed between first conjugation (t_{Seek}) and tumor cell apoptosis (Annexin V staining)
$t_{Contact}$	Cumulative duration of conjugation between t_{Seek} and t_{Death}
AR	Aspect ratio of polarization represented as the ratio of the major and minor axes of the cell, fitted to an ellipse
d_{Well}	Net displacement of the T-cell centroid, within the nanowell, averaged over 7 minute intervals
t_{AICD}	Time to effector cell death
Single killer	CAR^+ T cells that kill tumor cell at an E:T ratio of 1:1
Multi-killer	CAR^+ T cells that kill at least two tumor cells at an E:T ratio of 1:2-5
GzB	Granzyme B
AFU	Arbitrary fluorescence units

Supplementary methods

Image processing and Cell Segmentation: In order to permit accurate computation of cell displacements despite camera and stage movements, the individual nanowells were detected automatically with >99% accuracy by correlating pre-constructed shape templates at the expected range of orientations and magnification values. The correlation value is a maximum at the well centers, and these points are detected using a local maxima clustering algorithm. The cells in each image channel are analyzed automatically using a 3-step method[1]. First, each pixel is stratified as bright foreground, intermediate foreground, and dark background based on modeling image intensities as a mixture of three Gaussian distributions. The foreground pixels are subjected to multi-level thresholding (we used 10 equally-spaced levels between the maximum and minimum foreground intensity values). The cell centers are detected using a local maxima clustering on the average of Euclidean distance maps computed at each threshold. Using these cell centers, the image foreground is partitioned into individual cell regions using the normalized cuts algorithm, allowing cell sizes and shapes to be quantified. Spectral overlap between the dyes used under the imaging conditions were eliminated during image processing through our automatic "unmixing" process, and this is performed independently for each set of experiments. In addition, the segmentation scripts calculate an integrated fluorescence intensity by averaging on all the pixels associated with a given cell and thus eliminated any ambiguity in effector/target classification due to the diffusion of dyes across the cell membrane during contact.

Cell tracking: The detected cells, denoted $C_{i=1..N}^{t=1...T}$, where N is the number of cells in the well and T is the number of frames, are tracked from frame to frame using a graph-theoretic edge selection algorithm on a directed graph where cells correspond to vertices and edges represent

temporal association hypotheses[2]. The association cost for each edge $f_{i,j}^t$ between object i at time t and object j at time $t + 1$ is calculated based on cell location and size. The temporal correspondences are identified using an integer programming algorithm that maximizes the total association cost subject to constraints to ensure that each cell in a given frame is associated with a maximum of one cell in the subsequent frame, and vice versa.
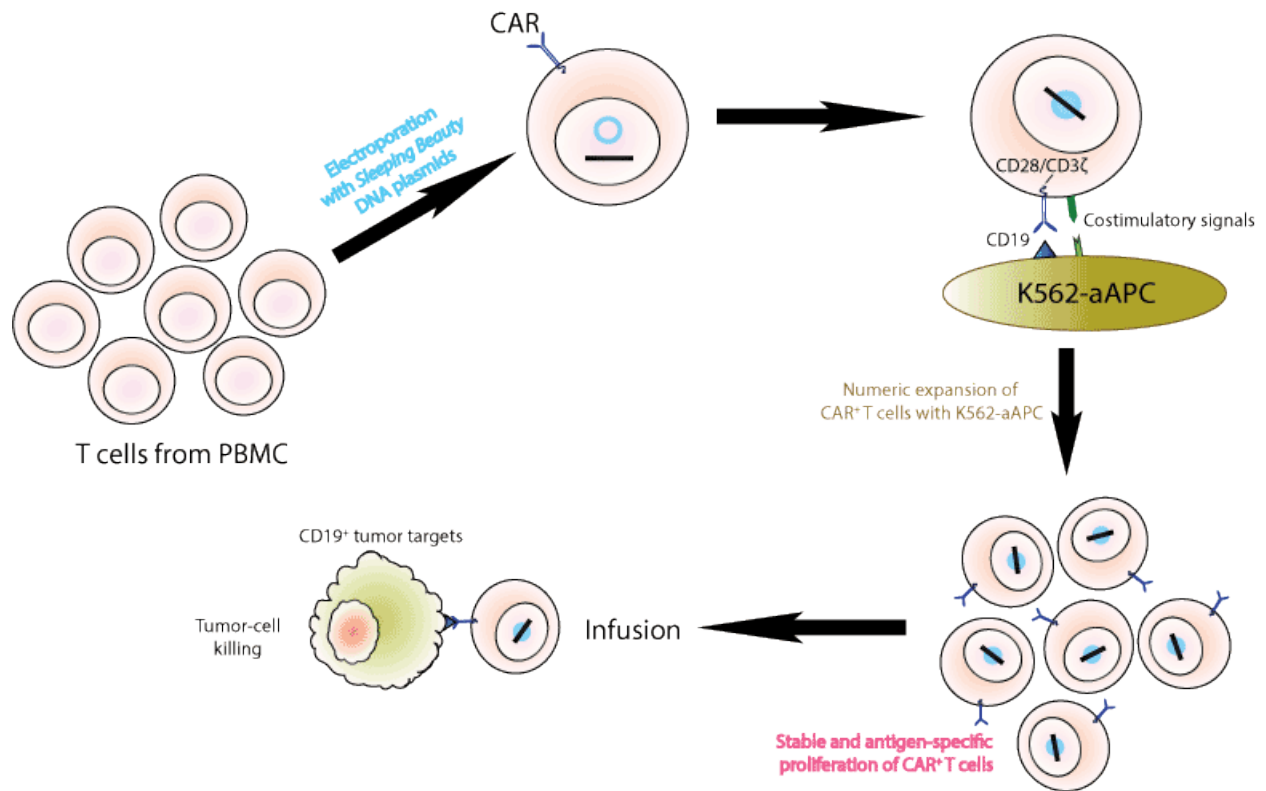
Figure S1. Genetic modification and expansion of CAR^{+} T cells. Peripheral blood mononuclear cells (PBMC) were electroporated with plasmids encoding for the Sleeping Beauty (SB) transposase and the transposon containing the CAR. The electroporated cells were subsequently expanded by co-culture with K562-derived artificial antigen presenting cells (aAPC) modified to express CD19, CD64, CD86 and CD137L, in the presence of exogenous IL-21 and IL-2.
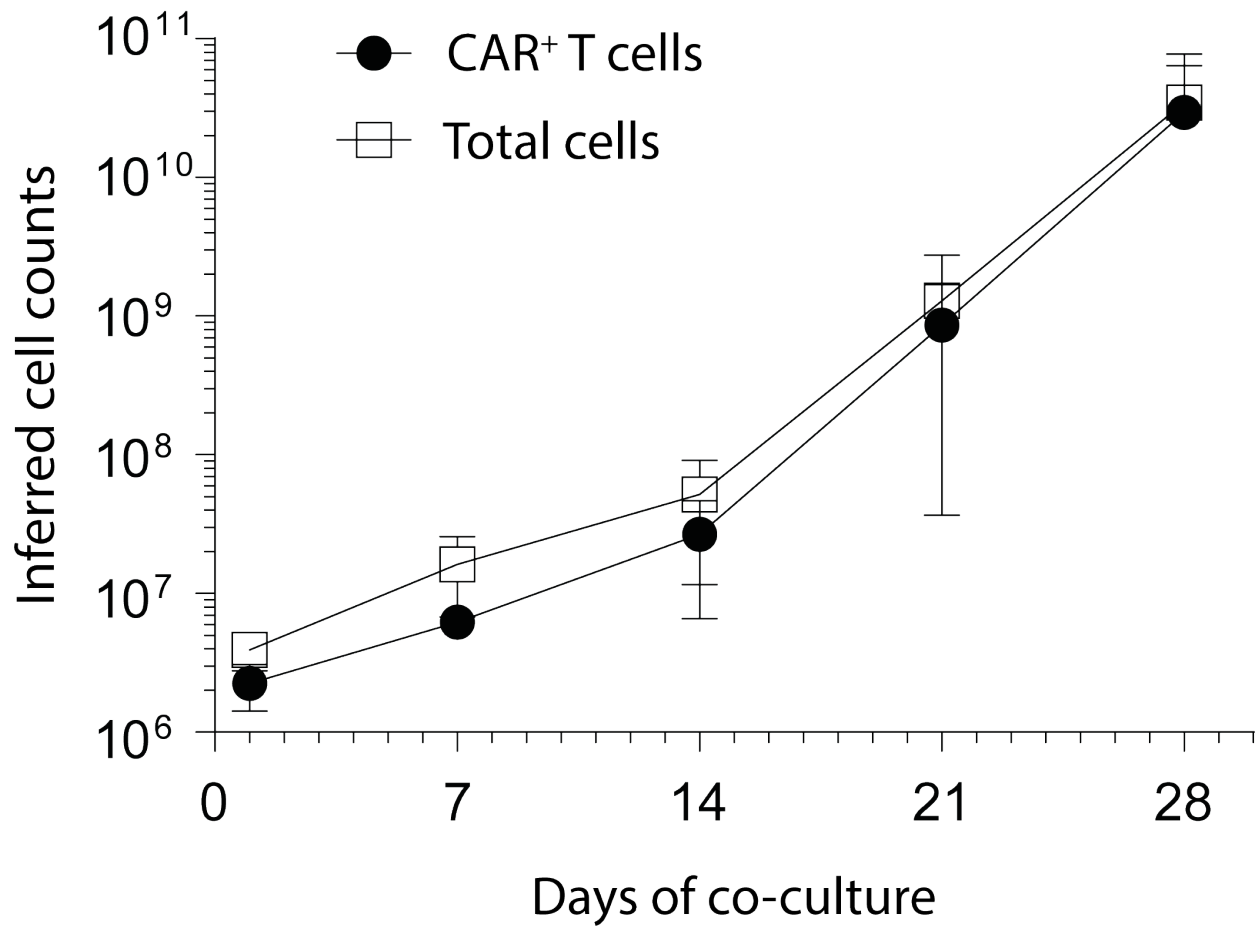
Figure S2. Representative data from a single donor showing expansion of CAR^+ T cells on aAPC in the presence of soluble IL-21 and IL-2. CD19RCD28 T cells showed $>10^4$ fold expansion in culture over a period of 4 weeks. Inferred cell counts were calculated assuming all viable cells were carried forward through each stimulation cycle. The error bars represent standard deviation from three independent measurements.
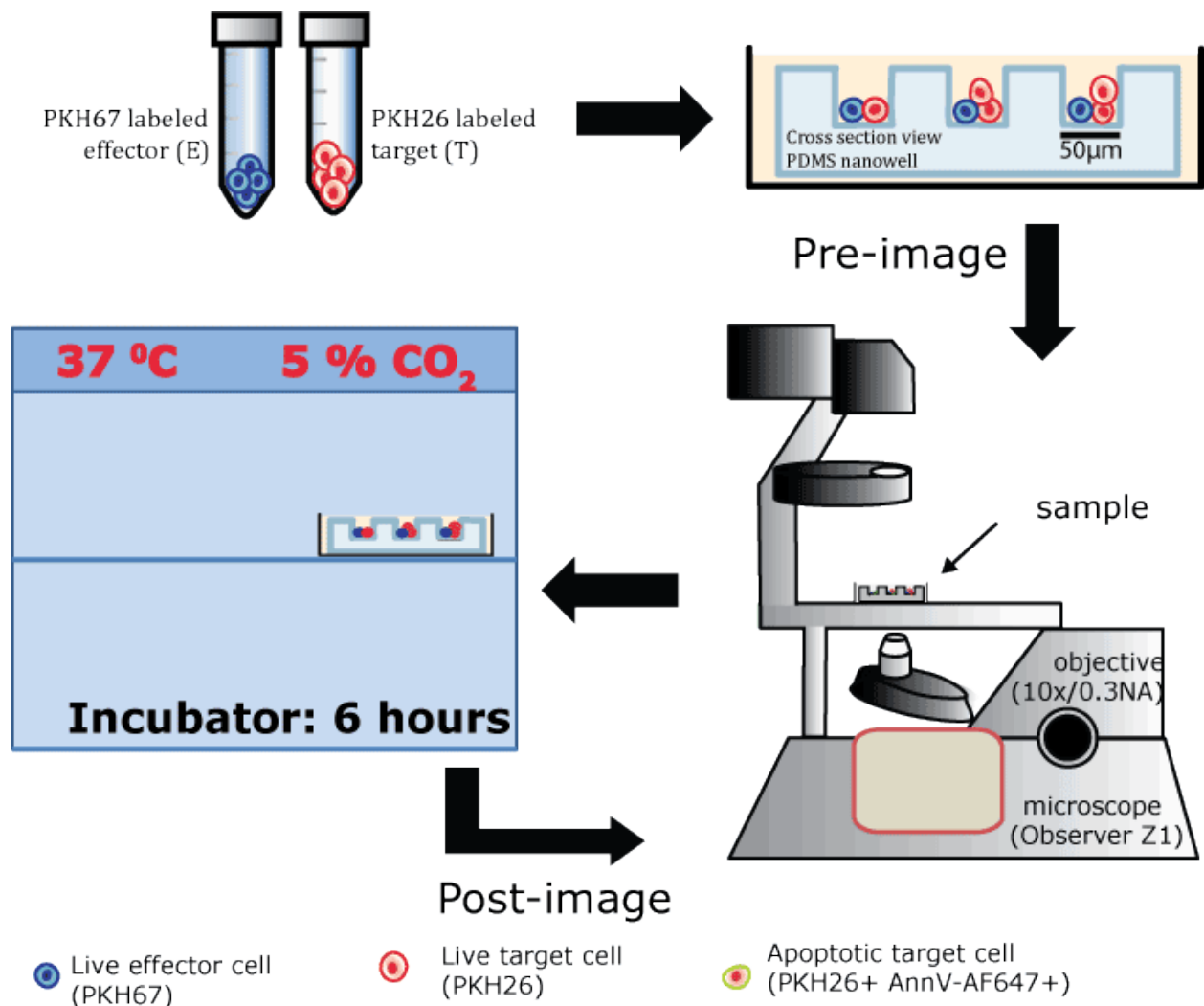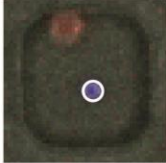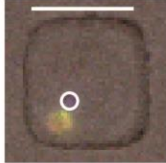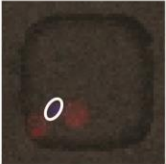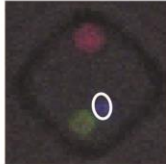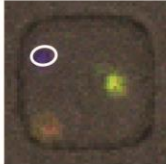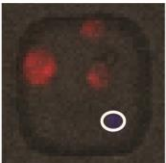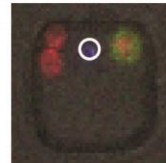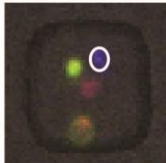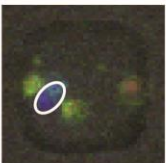
Figure S3. High-throughput cytotoxicity assay for monitoring T-cell target cell interactions in nanowell grids. Labeled effectors and target cells are loaded onto a nanowell array (~85,000 individual wells, 125pL each well) to enable monitoring of T-cell function at the single-cell level. Subsequent to loading and washing steps, the entire chip is immersed in cell-culture media containing AnnexinV. A pre-image is acquired on the microscope to determine the occupancy of every single nanowell and to exclude cells dead at the start of the assay. The array is then transferred to the incubator for 6 hours to enable cell-cell interactions and a second post-image is acquired. In house image segmentation programs are used to automatically process the images and database matching is employed to determine killing. In parallel, a separate nanowell array is loaded with targets only to determine the death rate in the absence of effectors, over the same period of time. The killing assay results are corrected for the background killing rate determined by the target only arrays.
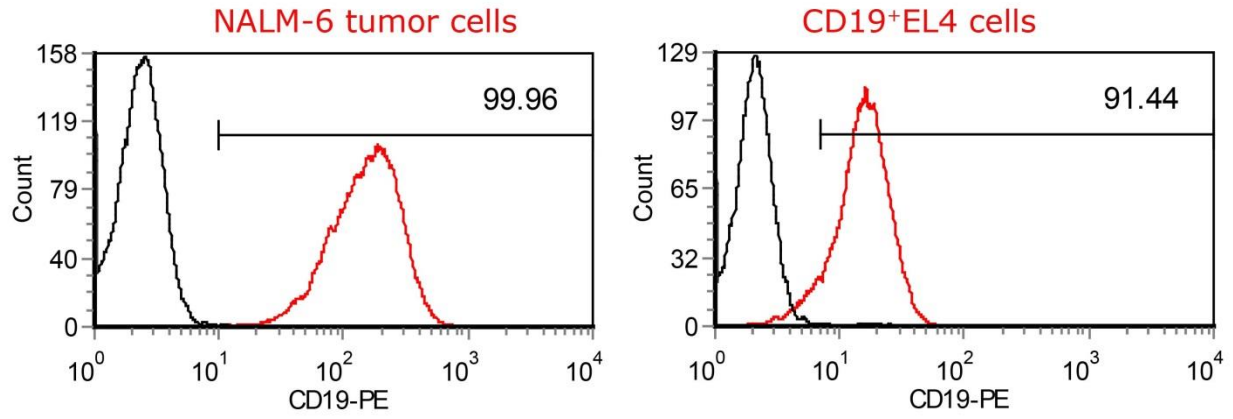
Figure S4. CD19 expression on NALM-6 tumor cells or CD19+EL4 target cells as determined by immunofluoresecent staining. The parental EL4 cell line was used as a negative control (black lines).

Number of Targets	Possible outcomes			
	0 killed	1 killed	2 killed	3 killed
1				
2				
3				

Figure S5. Composite micrographs illustrating representative examples of the interactions between single CAR^{+} T cells (E) and one or more NALM-6 tumor (T) cells. The tumor-cells are colored red, the CAR^{+} T cells are labeled blue with an artificial white exterior. Killing is determined by the colocalization of Annexin V staining (green) on red target cells. Scale bar 50 μm.
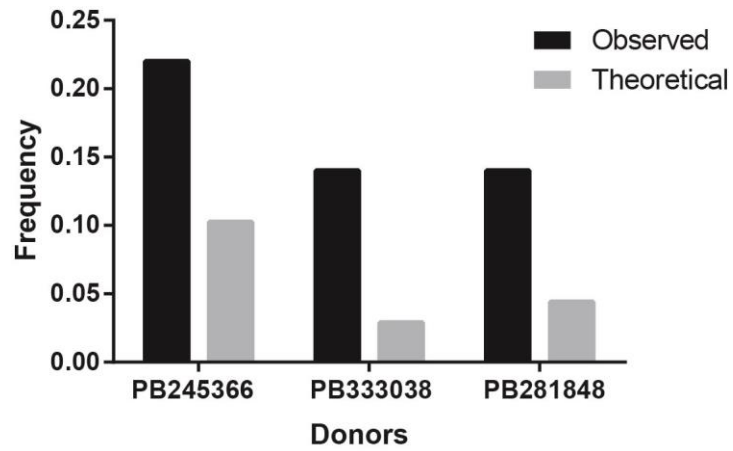
Figure S6. Increased probability of killing by individual CAR^{+} T cells at higher target cell densities. Comparisons of the observed killing frequencies at an E:T ratio of 1:2, and theoretical frequency, defined as the square of the frequency of killing at E:T of 1:1, assuming independence.

NALM-6 target cells
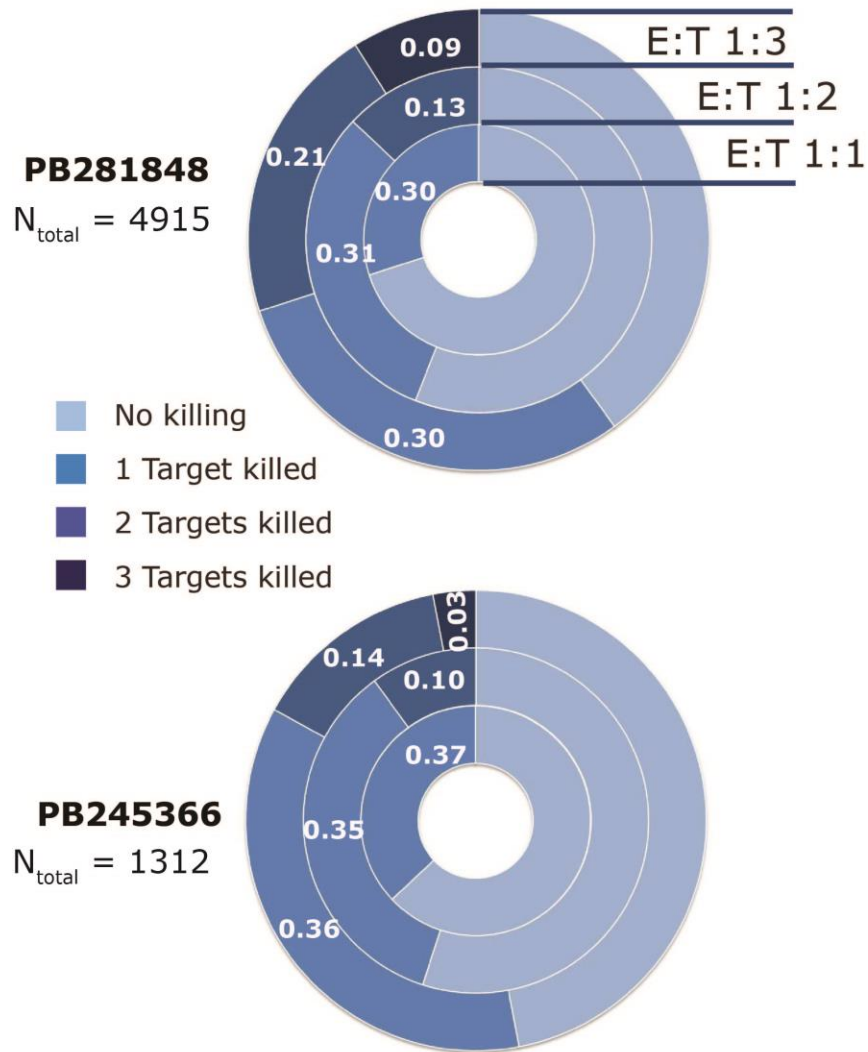
Figure S7. Donut plots summarizing the outcomes of the interaction between individual CAR8 cells and 1-3 CD19^{+}–NALM-6 tumor cells.
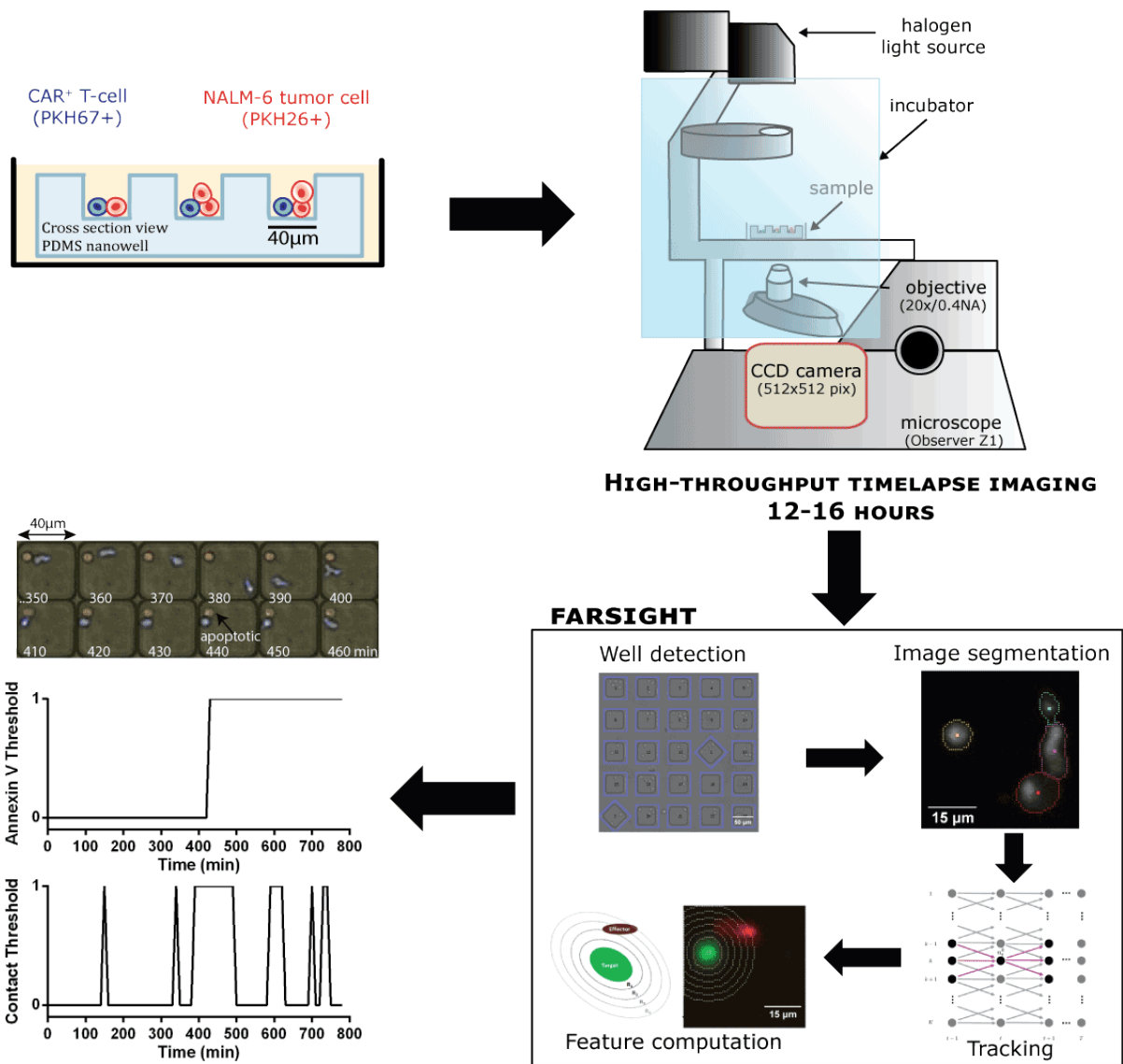
Figure S8. Timelapse Imaging Microscopy In Nanowell Grids (TIMING). PDMS nanowell arrays (64 pL each nanowell) are fabricated to bond a 60mm petridish. Labeled effectors and targets are loaded onto the nanowell array and the entire chip is immersed in cell-culture media containing fluorescent Annexin V. At least 6,000 nanowells are imaged every 7-10 minutes on the microscope for a total of 12-16 hours. Subsequently, an integrated pipeline within FARSIGHT is implemented to automatically enable well detection, image preprocessing and cell segmentation, tracking and feature computation. The images are fragmented such that each nanowell represents a single time series file. When analyzing time series data, only nanowells that yielded the exact same number of effectors and targets in >95% of time points were carried forward for analysis. Finally, the data is presented as time-series plots for each well along with the associated cell feature graphs.

12
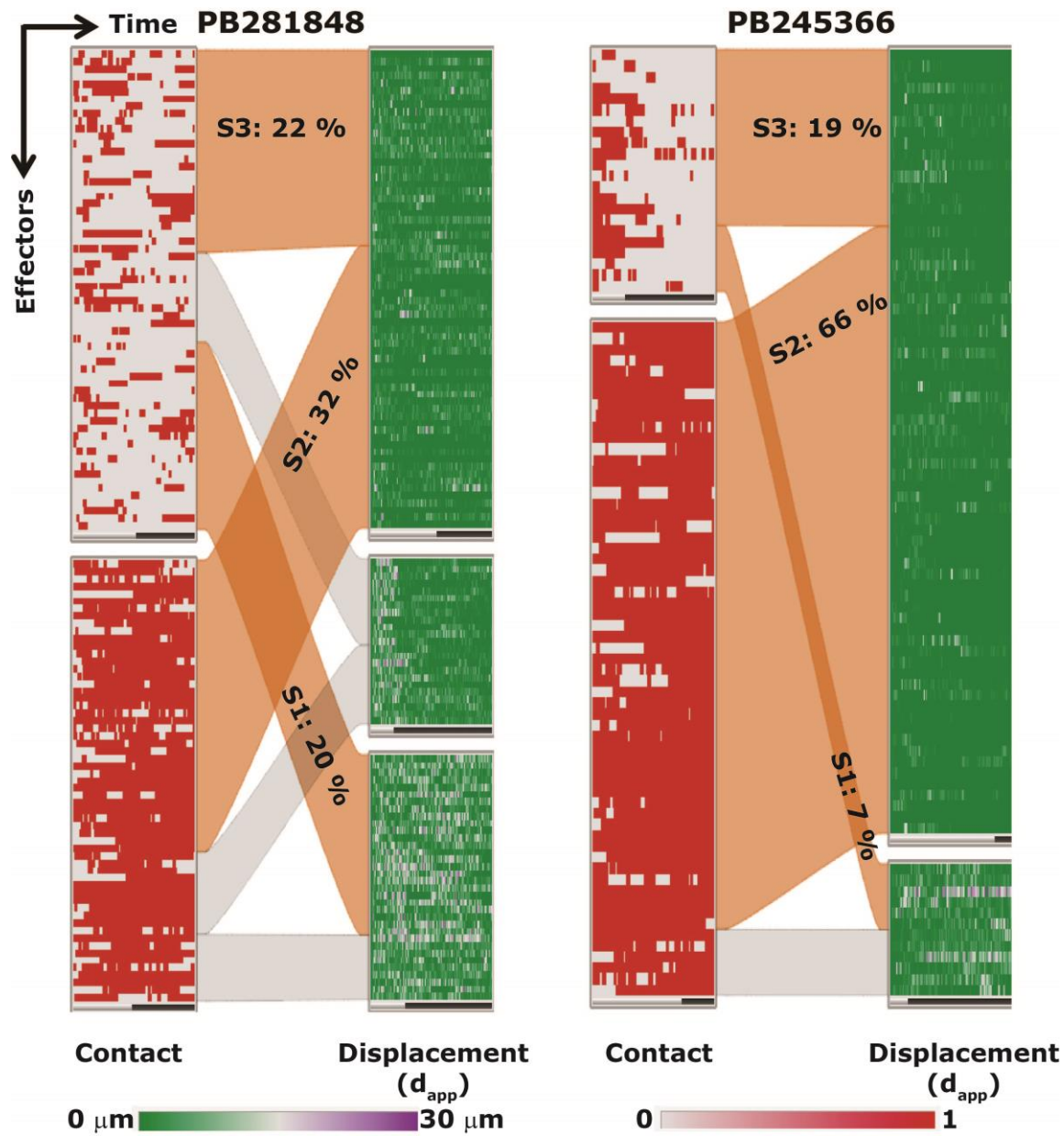
Figure S9. At an E:T ratio of 1:1, identification of subgroups of killer CAR8 cells based on their motility and contact behavior with tumor cells,. (A) The time series of the contact pattern of CAR8 cells in their interaction with NALM-6 cells was clustered using K-means clustering (Euclidean distance, complete linkage) to identify low and high contact duration subsets. The displacement (d_{well}) of the CAR8 cells was independently clustered to yield two or three subsets using K-means (Euclidean distance, complete linkage). Since these are features of the same cells, Caleydo was used to visualize the linkage between the clusters (gray cables) at single-cell resolution. The frequency of each of the three subsets, S1-S3, is highlighted in orange.
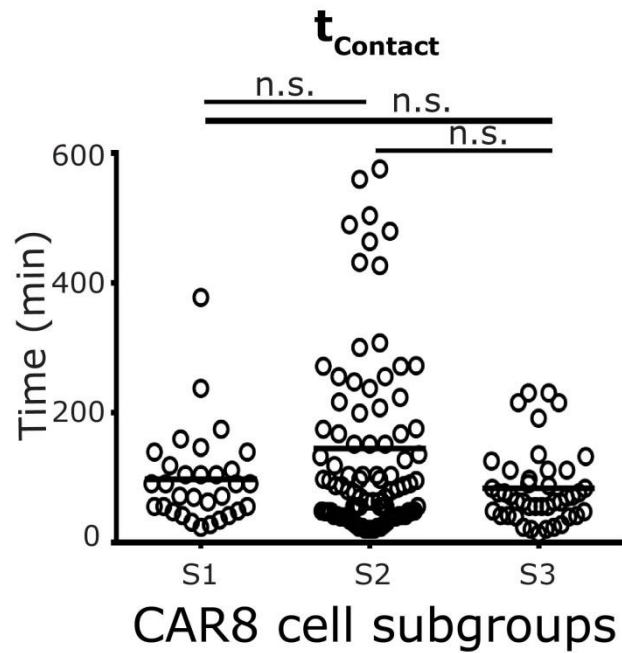
Figure S10. At an E:T of 1:1, the total duration of conjugation prior to NALM-6 tumor cell killing is no different for the CAR8 cells in the different subgroups. Each circle represents a single-cell and the horizontal black line designates the mean of the population. P-values were determined by parametric one-way Anova.
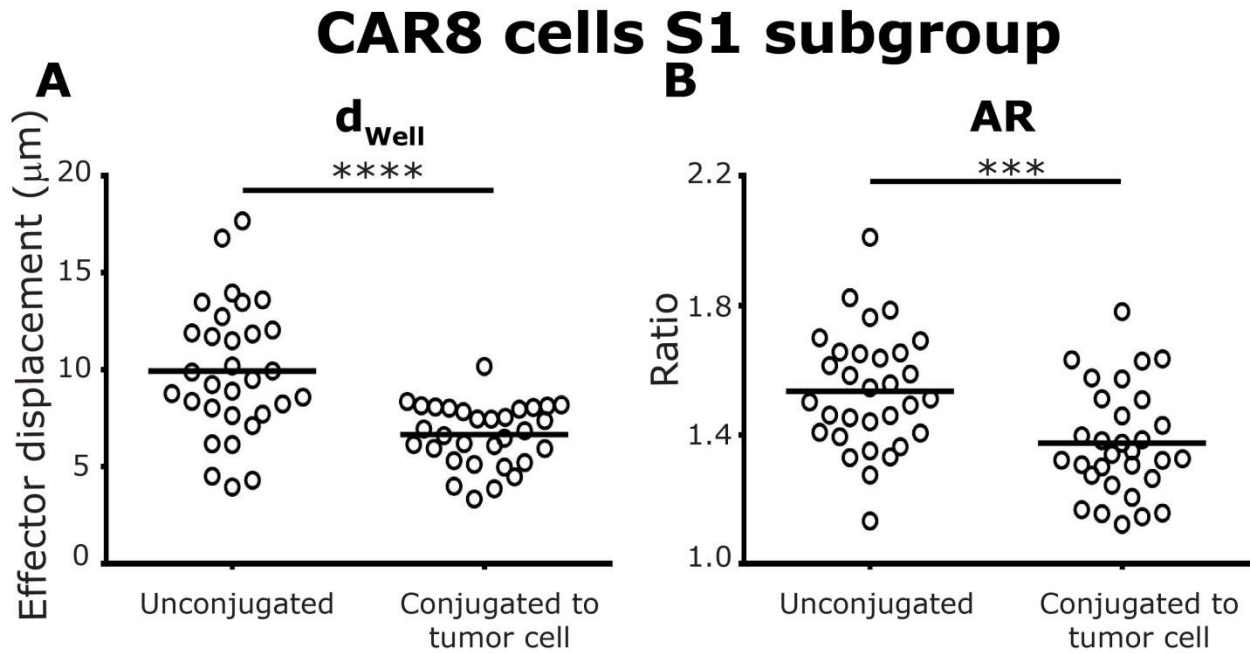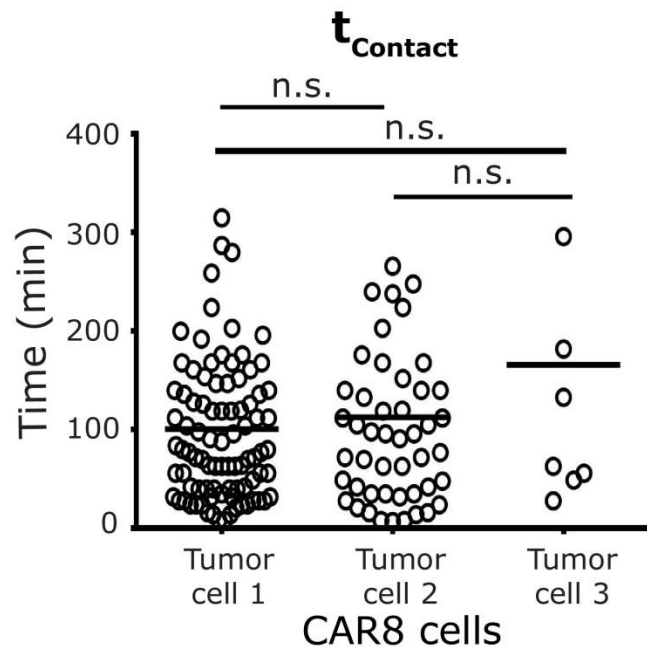
Figure S11. At an E:T ratio of 1:1, CAR8 cells in the S1 subgroup, demonstrate: (A) drop in motility, and (B) increased circularization upon conjugation to NALM-6 tumor cell. Each circle represents a single-cell and the horizontal black line designates the mean of the population. P-values were determined using a pairwise two-tailed t-test.

Time to effector apoptosis (t_{AICD})

| Frequency of AICD	
S1	17 %
S2	88 %
S3	53 %
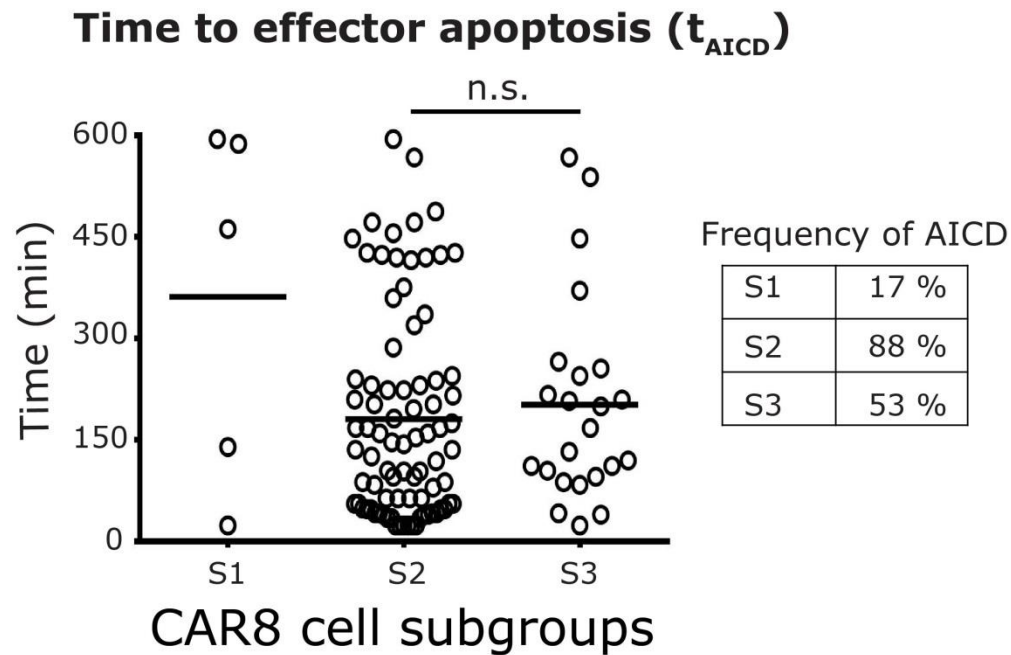
Figure S12. At an E:T ratio of 1:1, CAR8 cells in the different subgroups demonstrate different frequencies and kinetics of AICD subsequent to the interactions with NALM-6 cells. Each circle represents a single-cell and the horizontal black line designates the mean of the population. P-value was determined using a pairwise two-tailed t-test, and the S1 subgroup was excluded from testing due to the low number of apoptotic effectors.

Figure S13. At an E:T ratio of 1:2-5, multi-killer CAR8 cells demonstrate no significant differences in their duration of conjugation prior to killing multiple NALM-6 tumor cells. Each circle represents a single-cell and the horizontal black line designates the mean of the population. P-values were determined by parametric one-way Anova.

## Motility of CAR8 cells while conjugated to tumor cell
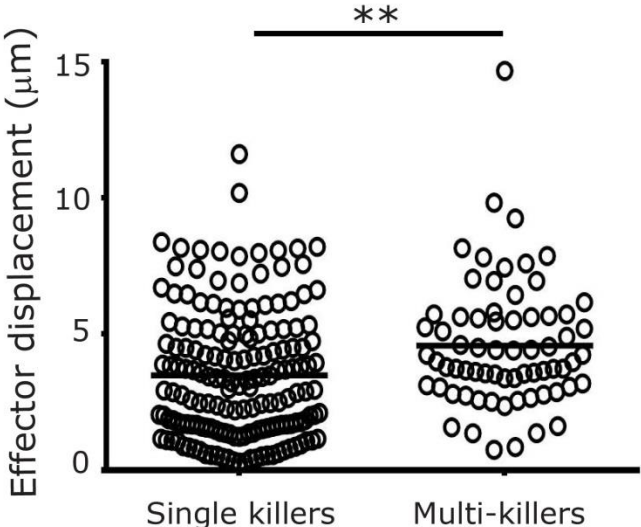
Figure S14. Despite the increased crowding because of higher tumor cell density, multi-killer CAR8 cells displayed greater motility when conjugated to tumor cell in comparison to single-killer CAR8 cells that encountered only a single tumor cell. Each circle represents a single-cell and the horizontal black line designates the mean of the population. P-value was determined using a pairwise two-tailed t-test.
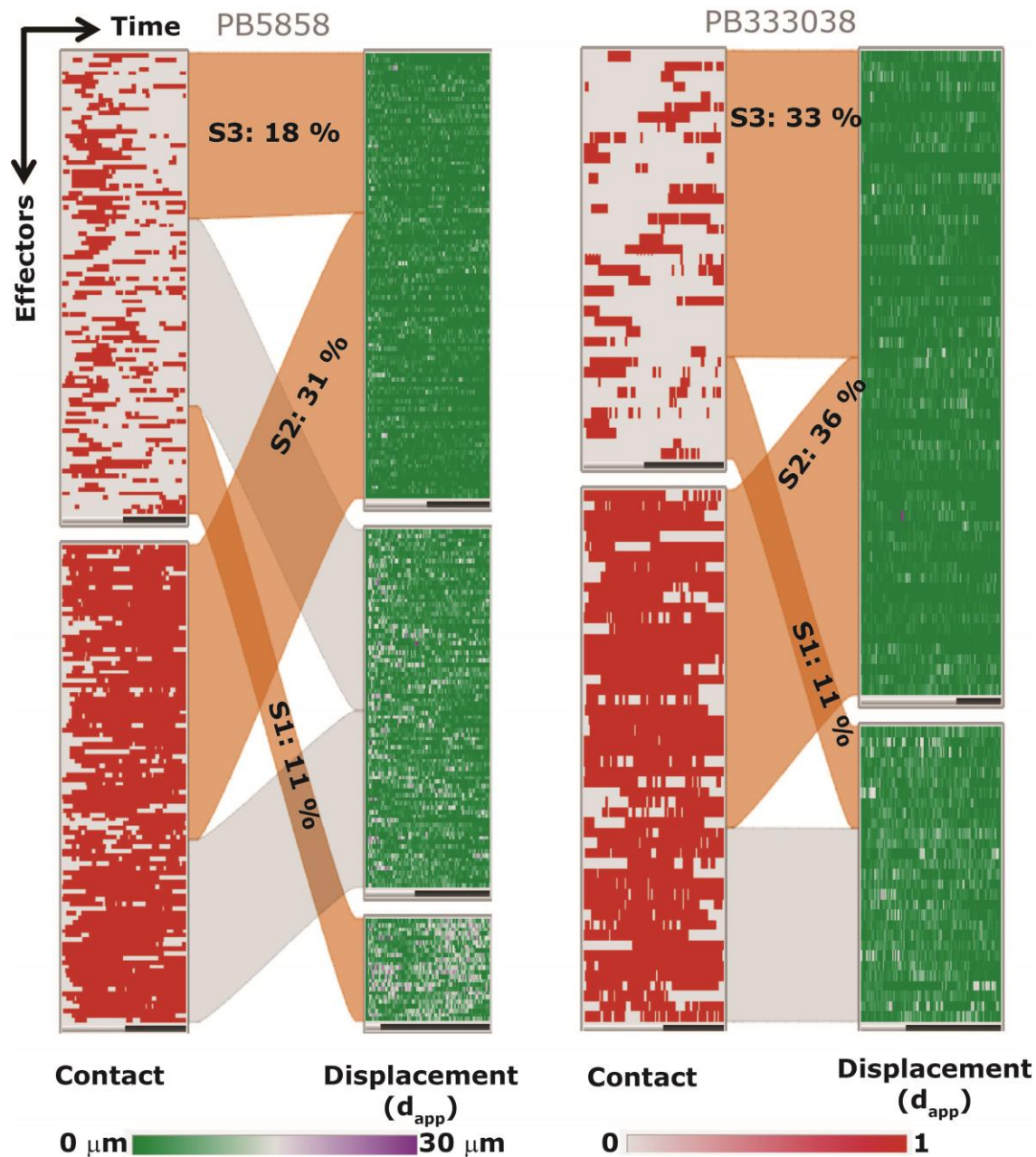
Figure S15. At an E:T ratio of 1:1, identification of subgroups of killer CAR4 cells based on their motility and contact behavior with tumor cells,. (A) The time series of the contact pattern of CAR4 cells in their interaction with NALM-6 cells was clustered using K-means clustering (Euclidean distance, complete linkage) to identify low and high contact duration subsets. The displacement (d_{well}) of the CAR4 cells was independently clustered to yield two or three subsets using K-means (Euclidean distance, complete linkage). Since these are features of the same cells, Caleydo was used to visualize the linkage between the clusters (gray cables) at single-cell resolution. The frequency of each of the three subsets, S1-S3, is highlighted in orange.
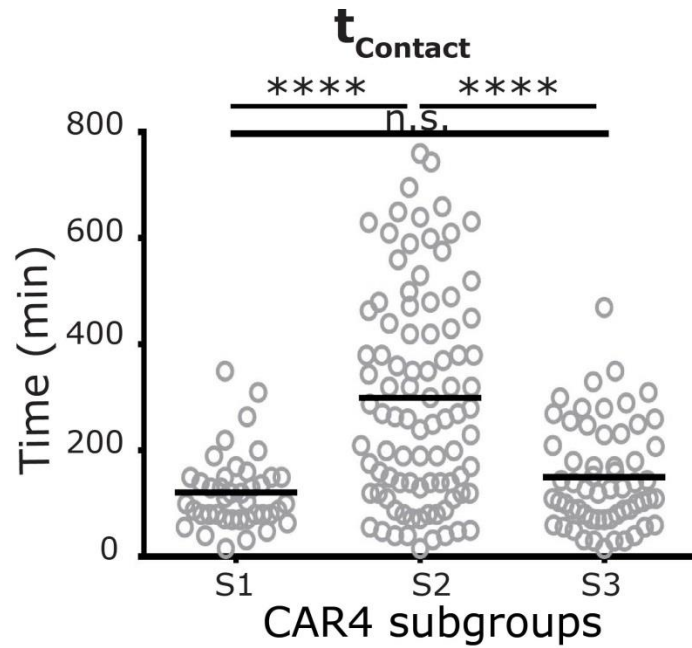
Figure S16. At an E:T of 1:1, the total duration of conjugation prior to NALM-6 tumor cell killing is significantly longer for CAR4 cells in S2 subgroup in comparison to subgroups S1 and S3. Each circle represents a single-cell and the horizontal black line designates the mean of the population. P-values were determined by parametric one-way Anova.
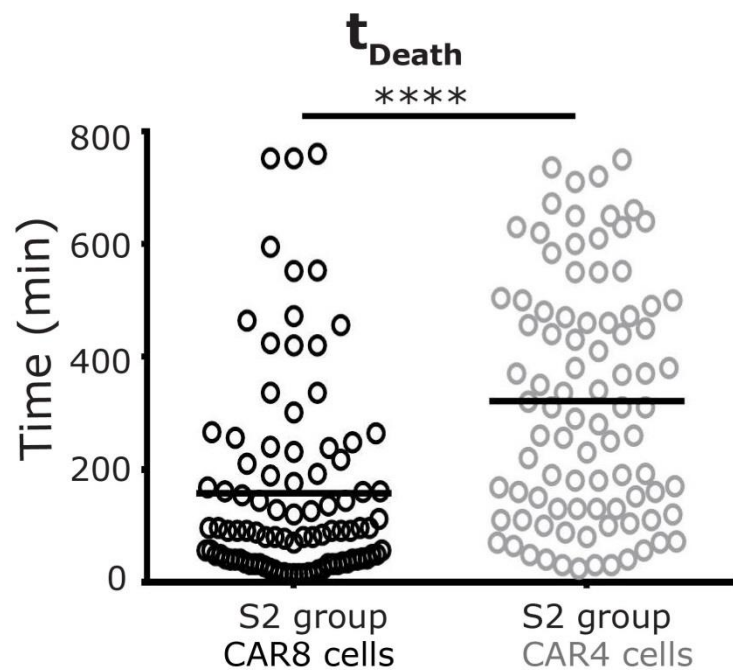
Figure S17. At an E:T of 1:1, CAR4 cells in S2 subgroup induce apoptosis in tumor cells with delayed kinetics in comparison to CAR8 cells in the S2 subgroup. Each circle represents a single-cell and the horizontal black line designates the mean of the population. P-value was determined using a pairwise two-tailed t-test.
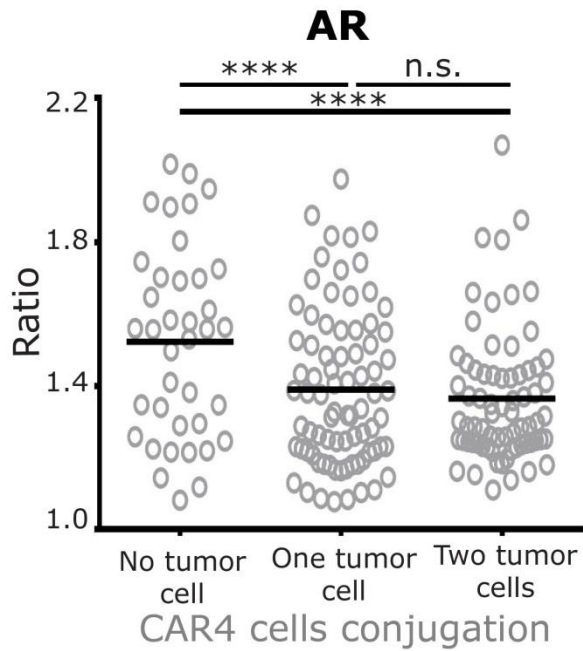
Figure S18. At an E:T ratio of 1:2-5, multi-killer CAR4 cells demonstrate increased circularization upon contact with one or more NALM-6 tumor cells. Each circle represents a single-cell and the horizontal black line designates the mean of the population. P-values were determined by parametric one-way Anova.
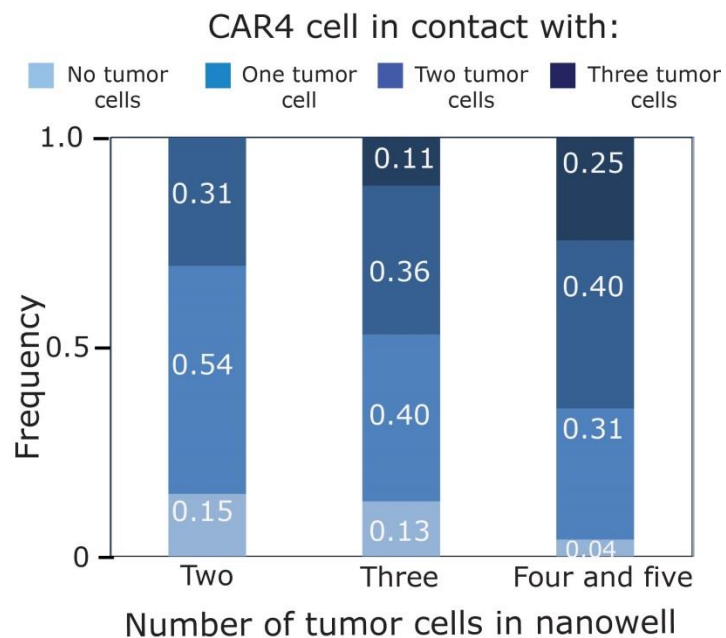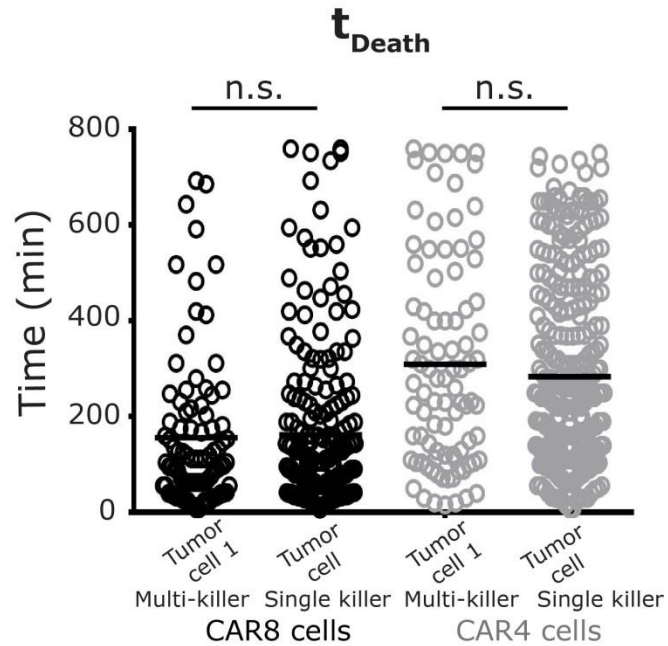
Figure S19. The ability of individual CAR4 cells to simultaneously conjugate to multiple NALM-6 tumor cells increases as the number of tumor cells within the nanowell increases.

Figure S20. Comparison of the killing efficiency of individual single killer CAR^{+} T cells (E:T 1:1) with multi-killer CAR^{+} T cells (E:T 1:2-5) that killed multiple NALM-6 tumor cells. The lack of difference in the killing efficiency within either the CAR4 or CAR8 population probably indicates that the formation of multiple conjugates by CAR^{+} T cells does not delay the kinetics of killing. Each circle represents a single-cell and the horizontal black line designates the mean of the population. P-value was determined using a two-tailed t-test.

REFERENCES

1   Luisi, J., Narayanaswamy, A., Galbreath, Z. & Roysam, B. The FARSIGHT trace editor: an open source tool for 3-D inspection and efficient pattern analysis aided editing of automated neuronal reconstructions. *Neuroinformatics* **9**, 305-315, doi:10.1007/s12021-011-9115-0 (2011).

2   Arunachalam Narayanaswamy *et al.* Multi-temporal Globally-Optimal Dense 3-D Cell Segmentation and Tracking from Multi-photon Time-Lapse Movies of Live Tissue Microenvironments. *Lecture notes in computer science* **7570**, 147-162 (2012).